Paper ID APEN-MIT-2022_4338
Applied Energy Symposium: MIT A+B
July 5-8, 2022 • Cambridge, USA

Dynamic and Steady-State Investigation of The Band Energy Distributions and Electronic Properties of Cu_2ZnSnS_4 and $Cu_2ZnSnSe_4$ Nanocrystals Utilizing Electrochemical Techniques

Bo Hou*

*School of Physics and Astronomy, Cardiff University, Queen's Buildings - North Building, 5 The Parade, Newport Road, Cardiff, CF24 3AA, United Kingdom. Email: Houb6@cardiff.acc.uk

Abstract— Quaternary chalcopyrite semiconductors, Cu_2ZnSnS_4 (CZTS) and $Cu_2ZnSnSe_4$ (CZTSe), have attracted increasing attention for photovoltaics (PV) application in recent years. However, due to the cell architecture borrowed from $CuIn_xGa(1-x)Se_2$ (CIGS) devices, the open-circuit voltage is the limiting factor preventing further increases in solar cell efficiency. In the present study, band edge energies of Cu_2ZnSnS_4 and $Cu_2ZnSnSe_4$ were analysed electrochemically in order to show band energy alignments of CZTS and CZTSe. The electrochemical steady-state potential windows were also investigated; this provides vital information for various applications of both materials. The valence band energy offset between CZTS and CZTSe was found to be 0.5 eV. Compared with the flat band potential of CdS (-0.8 V vs Ag/AgCl), the open circuit potential in the dark between CZTS and CdS is therefore 0.4 V and 0.9 V for CZTSe. Moreover, from chronoamperometric measurements using an electrochemical field-effect transistor, the conductivity of CZTSe is found to be three orders higher than CZTS, which proves that CZTSe is significantly better for charge transfer.

Keywords— chalcopyrite, Cu_2ZnSnS_4, $Cu_2ZnSnSe_4$, solar cells, electrochemical field-effect transistor

Introduction

Quaternary chalcopyrite semiconductors, Cu_2ZnSnS_4 (CZTS) and $Cu_2ZnSnSe_4$ (CZTSe), which crystallize in a double cubic superlattice (kesterite, named after the mineral $Cu_2(Zn, Fe)SnS_4$), have attracted increasing attention for photovoltaic (PV) applications in recent years.[1-6] Device efficiencies of CZTS(Se) cells have increased rapidly above 12%.[7, 8] However, due to the cell architecture (based on copper indium gallium selenide/sulfur [CIGS] technology: Mo substrate, CdS, ZnO, CZTS(Se) further progress is likely to be limited.[9] Mitzi and Walsh's comparison between CZTS(Se) with CIGS solar cells concludes that the cells generate similar currents, but the limiting factors for CZTS are the open-circuit voltage deficit and point defects.[10-16] Computational modelling has been used to provide much of the band structure data for CZTS and CZTSe, however, a systematic steady and dynamic electrochemical analysis of CZTS and CZTSe, as well as what is their conductivity difference and electrochemical band alignment, is still lacking within the community.[17-22] Moreover, the electrochemical steady-state potential windows of CZTS and CZTSe provide important information about the limitations of various Net Zero applications, including solar cells, CO_2 photoreduction, water splitting and lighting.[4] Therefore, understanding the band structure, such as band energy levels, conductivity properties, and band edge offset, is paramount for enhancing and deploying CZTS(Se) materials into energy-efficient applications.

Herein, the redox properties of CZTS and CZTSe nanocrystals which relate to the band structures, are analysed electrochemically. First, by utilizing cyclic voltammetry (CV), electrochemical potentials can be applied to the modified gold electrode to obtain the potential at which the system switches between capacitive and faradaic behaviour. Then, by employing an electrochemical field-effect transistor, the electron transfer abilities of CZTS and CZTSe can be investigated in the capacitive region obtained from the CVs.

I. Experimental Details

Synthesis of CZTS and CZTSe nanocrystals. The syntheses of CZTS (Cu_2ZnSnS_4) and CZTSe ($Cu_2ZnSnSe_4$) nanocrystals were performed using the hot-injection method as previously reported.[23] A typical procedure was as follows: 1.5 mmol (0.39264 g) of copper(II) acetylacetonate (99.99 %, Aldrich), 0.75 mmol (0.1977 g) of zinc acetylacetonate hydrate (99.995 %, Aldrich), and 0.75 mmol (0.2909 g) of tin (IV) bis(acetylacetonate) dichloride (98 %, Aldrich), and 10 ml of oleylamine (technical grade, Aldrich) is added into a 100 ml three-neck flask connected to a Schlenk line (all the chemical were used directly without any further purification). The mixture is heated to ~130 °C under vacuum for 30 minutes before being raised to 250°C. Then, the whole system changed to the Ar condition where 3 ml of 1M solution of sulfur in oleylamine (0.6414 g sulfur dissolved into 20 ml oleylamine) or 3 ml of 1M solution of selenium in oleyamine (1.5792 g selenium dissolve into 20ml oleylamine by heating at 200 °C overnight) is injected. After injection, the colour of the solution turns from darker brown to black after holding the temperature at 225°C for 30 minutes. The mixture was

then cooled to ~80 ºC, and 5 ml toluene and 40 ml isopropanol was added to the reaction solution and centrifuged for purification. The final precipitate was dispersed into toluene.

X-ray powder diffraction pattern (Bruker D8) was achieved by putting the powder of CZTS or CZTSe on silicon wafer sample holders. The lattice spacings of CZTS and CZTSe nanocrystals were achieved by averaging measurements from multiple fringes. The measurement result was 0.31 nm which corresponds to the CZTS d_{112} crystal plane, and 0.32 nm in the case of CZTSe. The composition of CZTS and CZTSe were determined by EDX from HRTEM (JEOL TEM 2010, Oxford Instruments ISIS 300 system) and SEM element mapping (JEOL JSM 5600LV). Typically, the purified CZTS and CZTSe were dissolved into toluene for HRTEM and EDX analysis, after the HRTEM analysis, the same TEM grids were put on the aluminium holder for EDX mapping, which was performed on SEM (JEOL JSM 5600LV) with x-ray analysis suite (Oxford Instruments ISIS 300 system).

II. Results and Discussion

A. Optical property, crystalline structure, composition characterization.

UV-Vis-NIR spectra were extracted by dispersing the nanocrystals into toluene and measured at room temperature, as shown in Figure 1. The optical band gap (ε_g) of the materials was estimated by plotting $(\alpha h\nu)^2$ as a function of the photon energy. From the estimation, the εg of CZTS is 1.5 eV which coincides with the reported values, but the ε_g of CZTSe is 1.7 eV which is bigger than the reported values.[4, 8, 24] Since we calculated the bandgap of the CZTSe spectrum cut before the tale end, which may result in the value of CZTSe being bigger than CZTS.[25] In order to further investigate the bandgap of these materials, a systematic electrochemistry analysis was performed in the following sections.

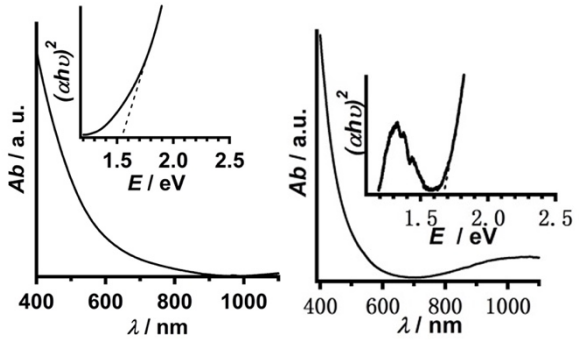

Fig.1. Room temperature UV-vis-NIR absorbance spectrum of CZTS(left) and CZTSe (right) nanocrystals dispersed in toluene. Insets show the estimated bandgap energies of CZTS (1.5 eV) and CZTSe (1.7 eV).

B. Growth, crystallography and morphology

Kesterite crystal structures were further confirmed by powder X-ray diffraction (XRD) and selected area electron diffraction (SAED), as shown in Figure 2 a,b and c. Both CZTS and CZTSe were found to be kesterite structure. After replacing S with Se, the diffraction peak showed a left shift, which indicated CZTSe had a bigger lattice distance than CZTS. By employing the well-defined peak from XRD (220_CZTS) and (204_CZTSe), SAED results and high-resolution transmission electron microscopy (HRTEM) measurements (Figure 1d), we calculated the lattice constants of CZTS *a*: 5.40 ± 0.02 Å, *c*: 10.8 ± 0.02 Å and CZTSe *a*: 5.64 ± 0.02 Å, *c*: 11.28 ± 0.02 Å. The lattice spacings of CZTS and CZTSe nanocrystals were achieved by averaging measurements from multiple fringes. The measurement result was 0.31 nm which corresponds to the CZTS d_{112} crystal plane, and 0.32 nm in the case of CZTSe. The extracted lattice parameters are close to the standard kesterite structure. Through Lorentzian fitting of the XRD results, as shown in Figure 1c, we calculated the crystal domain size of CZTS and CZTSe to be 29.1 ± 5.7 nm and 49.3 ± 4 nm using the Scherrer equation (average values of the three prominent peaks were taken), and these values are correlated well with the HRTEM results. As reported previously, the tiny extra peak in the XRD pattern (112) plane was assumed to come from crystal structure disorder.[15, 16] The compositions of CZTS and CZTSe were determined by scanning electron microscopy (SEM) element mapping, Energy-dispersive X-ray spectroscopy (EDX) measurement and HRTEM, as shown in Figure 3. The stoichiometric element ratio of CZTS and CZTSe was found to be $Cu_{0.25}Zn_{0.12}Sn_{0.14}S_{0.49}$ (close to the expected ratio of 2:1:1:4) and $Cu_{0.41}Zn_{0.06}Sn_{0.12}Se_{0.41}$ (~3.5:0.5:1:3.5 with Cu rich). The element mapping has shown that both materials have a homogenous quaternary element distribution without secondary phase separation.

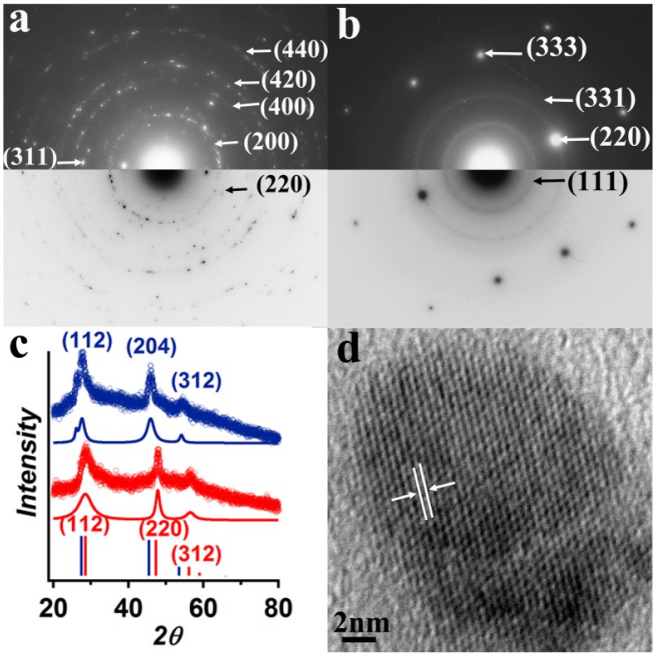

Fig. 2. a), b) SAED patterns of as-prepared CZTS and CZTSe nanocrystals. The camera length is 267 mm, and electron wavelength is 0.025 Å. c) XRD diffractograms (Cu Kα: λ=1.54Å) of as-prepared CZTS (bottom line) and CZTSe (top line) nanocrystals, the smooth lines below each diffraction pattern were achieved from Lorentzian fitting, the 2θ of CZTS (220) plane is 47.8º, and the 2θ of CZTSe (204) plane is 45.8º. PDF reference data for Kesterite structures of CZTS:00-026-0575, CZTSe:00-070-8930. d) HRTEM image of CZTS showing a lattice spacing for the (112) plane of 3.1Å.

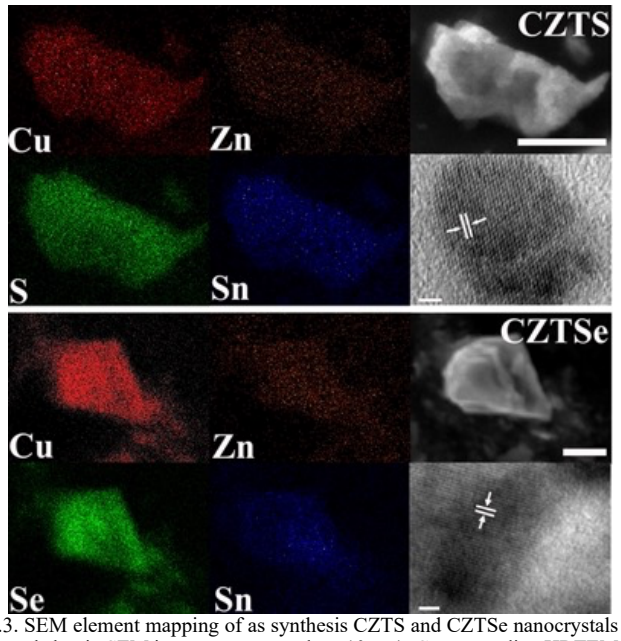

Fig.3. SEM element mapping of as synthesis CZTS and CZTSe nanocrystals (the scale bar in SEM images corresponds to 10 nm); Corresponding HRTEM images of the nanocrystals measured in SEM, the lattice spacing of (112) plane related to CZTS is 3.1 ± 0.02 Å and 3.2 ± 0.02 Å to CZTSe (the scale bar in HRTEM is 2 nm).

C. *Cyclic voltammetry analysis*

Electrochemical techniques such as CV measurements are useful for measuring the effects of applied potentials; differencing scan rates can be used to investigate the materials' redox properties on the modified electrode. In this report, the working electrodes for the CVs were prepared by drop-casting CZTS or CZTSe nanocrystal solutions (2*20 µL, 20 mg ml^{-1}) onto gold electrodes. A 0.5 M KCl aqueous solution (PH=7) was chosen as a supporting electrolyte, and standard Ag/AgCl and Pt foil electrodes were employed as reference and counter electrodes, respectively. A series of CVs in different scan windows were performed on gold electrodes modified by CZTS or CZTSe, as shown in Figure 4. In Figure 4a, the solid colour line is attributed to the steady-state potential window (-0.3 V to -1.1 V) of CZTS. The stability was confirmed over 10 cycles scan. However, when biasing to a more positive potential, the capacitive effect was replaced by the faradaic current generated as shown in Figure 4a, the grey and red dashed lines. This implies the ionization potential (valence band edge) of CZTS is located at -0.4 V. But, due to the potential window being limited by hydrogen production, the conduction band edge of CZTS cannot be measured with the current setup. Combining the valence band position with the optical band gap of CZTS (~ 1.5 eV as shown in Figure 1), the conduction band edge of CZTS is predicted to be located at -1.9 V (vs Ag/AgCl).

In the same way, as shown in Figure 4b, the solid coloured line is attributed to the steady-state potential window of CZTSe (0.1 V to -0.6 V), which mainly shows capacitive current. However, when a more positive potential is applied (as in the red dashed line) or a more negative potential (triple colour dashed line in the inset graph in Figure 4b), the current switches from capacitive to a faradic current which is due to the decomposition of CZTSe (current is seen to decrease during three scans in the inset graph of Figure 4b). Thereafter, we confirmed the valence band edge of CZTSe is at 0.1 V, and the conduction band edge is located at -0.8 V (vs Ag/AgCl).

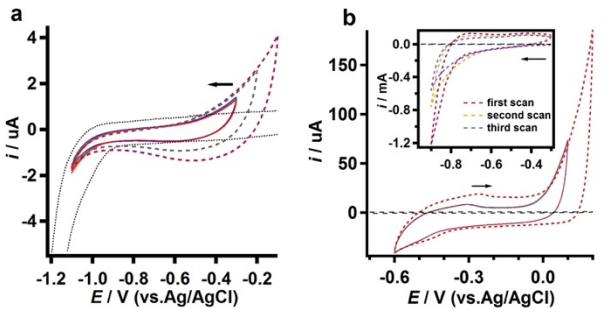

Fig. 4. Cyclic voltammograms of as-prepared CZTS (a) and CZTSe (b) in 0.5 M KCL at scan rate 0.05 Vs^{-1} on a gold electrode. The black arrow indicates the scan direction and starts potential, and the black dotted line is the background signal.

D. *Electrochemical field-effect transistor*

An electrochemical field-effect transistor is a device that uses an electrochemical gate to control electrical current flow between the source and drain electrodes.[26, 27] This effective gate leads to reversible switching between oxidized and reduced states in redox-active substances bridging the source and drain electrodes. The material is biased with respect to a reference electrode (electrochemical gate) inserted in the electrolyte, the conductance of the target material can then be measured as a function of the electron density of the redox states.[27] In the present work, the measurement setup was as shown in Figure 5. The working electrode used for the lateral conductivity measurements was an interdigitated electrode (IDE, as shown in Figure 5a), 50 digit pairs, 5mm long, with 20 µm finger and spacings widths purchased from ABTECH Scientific, Inc. CZTS and CZTSe nanocrystals dispersed in toluene (20 mg/ml) were drop-casted over the entire surface of the working electrode. An Ivium Compactstat bipotentiostat (Ivium Technologies) and conventional electrochemical cell (0.5M KCl aqueous solution, PH=7) with Ag/AgCl, Pt foil as a reference and counter electrodes were employed. The CZTS and CZTSe nanocrystals were assumed to assemble homogeneously over the IDE electrode, including the space between the digit pairs. Because of the CV results discussed above, the gating potential applied to the IDE varied from -1.3 to -0.1 V (CZTS) or -1.0 to 0.2 V (CZTSe) with respect to the Ag/AgCl reference electrode. The bias voltage between the source and drain varies from -0.02 to 0.02. For each gating potential, a 5 minute current transient with zero source-drain bias was recorded, and then a transient current was recorded for 30s at every bias potential; the gradient of current vs biasing potential provides a conductance, which can be multiplied by a cell constant of 0.04 cm^{-1} to calculate conductivity.

As shown in Figure 6a, the conductance of CZTS and CZTSe increases swiftly when the gate voltage applied reaches the expected band edge potentials, providing good evidence that they are indeed the band edge potentials. However, when the potential increases beyond the steady-state potential window, as discussed in the CV analysis, the faradaic current generated drives the electron flow into the electrolyte instead of through the film. Therefore, as shown in Figure 6a, the conductivity decreases (CZTSe blue curve) or increases (CZTS red curve). It should be noted that the conductivity of CZTSe is very high even within the bandgap (no electron flow would be expected within an intrinsic semiconductor). The difference between the conductivity at the band edge and within the bandgap is very small, and this is indicative of as-prepared CZTSe having a highly doped

nature. Since the elemental analysis results show Cu rich areas within the CZTSe nanocrystals, it is assumed the richer Cu provides excess charge carriers, and this may also explain why there is a tail in the absorption spectra (Figure 1). From the calculation results of Persson[19], the effective masses of holes in CZTS and CZTS show strong anisotropy, CZTSe has smaller hole masses than the corresponding CZTS. Persson also concluded that the CZTSe would expect to have a better response to an applied electric field.[19] Prieto and co-workers have also observed a similar phenomenon in the selenium effect of $Cu_2ZnSnS_{1-x}Se_x$ thin films.[28] After replacing S with Se, they found that the electrical conductivity of the as-prepared nanocrystals increased without annealing.[28]

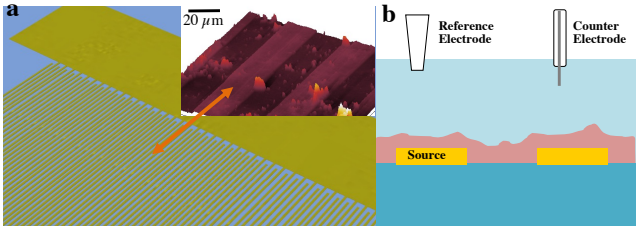

Fig. 5. a) Diagram of the interdigitated electrode, inset AFM image shows dilute sample bridging the two electrodes, full concentration samples entirely cover electrodes. b) Schematic of the electrochemical field-effect transistor measurement setup.

By adapting n-type CdS bulk single-crystal valence band edge (E_{VB}) as 1.62V vs Ag/AgCl and conduction band edge (E_{CB}) as -0.8V vs Ag/AgCl from our previous work,[29] we obtain the band alignment of CdS, CZTS and CZTSe as shown in Figure 6b. We found the open-circuit voltage between CZTSe and CdS is 0.5 V higher than CZTS vs CdS. This may explain why devices of CZTS have to change to CZTSe for high-efficiency performance in CIGS solar cell structures.[7] The valence band and conduction band positions of CZTS and CZTSe can be extracted from previous simulation results.[18] As shown in table 1, the experimental results were comparable to the calculated results. Scragg reported flat band potential values of CZTS reported by Scragg were located between -0.2 and 0.2 V (vs Ag/AgCl).[3, 30] Since the electrodeposited CZTS thin film was a p-type semiconductor, the flat band potential would be close to the valence band edge. The experimental band gap value of CZTSe is around 0.9eV (0.1eV less than the single crystals CZTSe values), which matches with previous reports [18, 22], which also attribute the p-type conductivity of CZTS and CZTSe to the Cu/Zn antisite(Cu_{Zn}) that give a 0.12 eV transition-energy level of Cu_{Zn} above the valence band maximum.[18]

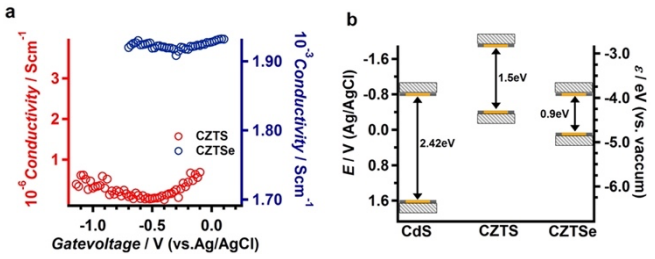

Fig. 6. a)Conductivity of CZTS (blue dot) and CZTSe (red triangle) nanocrystals as a function of applied potential. b) The band alignment between CdS, CZTS and CZTSe.

TABLE I. CORRELATION OF OPTICAL, COMPUTER SIMULATION, FLAT BAND POTENTIAL OF CZTS AND ELECTROCHEMICAL BAND GAPS, BAND EDGES FOR CZTS AND CZTSE NANOCRYSTALS

Method	E_{VB} CZTS	E_{VB} CZTSe	E_{CB} CZTS	E_{CB} CZTSe	ε_{gap} CZTS	ε_{gap} CZTSe	E_{VB} offset	E_{CB} offset
Absorption Spectrum	-	-	-	-	1.5eV	1.7eV	-	-
[a]Computer simulation	0.61V	0.46V	-0.89V	-0.54V	1.5eV	1.0eV	0.15V	-0.35V
CV experiment	-0.3V	0.1V	-1.8	-0.8V	1.5ev	0.9eV	-0.1V	-0.3V
Lateral conductivity measurement	-0.4V	0.1V	-1.9	-0.8V	1.5ev	0.9eV	-0.2V	-0.5V
[b]Flat band potential	0.2V	-	-1.29V	-	1.49eV	-	-	-
[c]Flat band potential	0V	-	-1.49V	-	1.49eV	-	-	-
[c]Flat band potential	-0.2V	-	-1.72V	-	1.52eV	-	-	-

[a.] Calculated from Shiyou's results[18]; [b] value was measured in 0.2M $Eu(NO_3)_3$ at pH=2.33. [c] values were derived from photocurrent vs bias potential measurements, and the measurement potential was chosen to correspond to the peak photocurrent.

III. CONCLUSION

In summary, solution-processed quaternary chalcopyrite semiconductors CZTS and CZTSe band edge energy levels, electrochemical steady-state potential windows and film conductivities were analysed electrochemically. We found that the valence band energy offset between CZTS and CZTSe is 0.5 eV. Compared with the flat band potential of CdS (-0.8 V vs Ag/AgCl), the open circuit potential in the dark for CZTS and CZTSe are 0.4 V and 0.9 V, respectively. Moreover, from chronoamperometric measurements using an electrochemical field-effect transistor, the conductivity of CZTSe is found to be three orders higher than CZTS, which suggests that CZTSe is significantly better for charge transport. Therefore, we believe CZTSe solar cell devices have better efficiencies than CZTS devices may also be attributable to the higher charge transportability and larger (0.5 eV) dark open-circuit voltage. Therefore, to further enhance the efficiency of CZTS devices, the most effective way is to find another layer to replace CdS and adjust the element ratios, especially the Cu to Zn ratio, which are expected to create better charge transport abilities and band alignments.

ACKNOWLEDGMENT

This research is supported by the Engineering and Physical Sciences Research Council (EP/G031088/1), SUPERGEN Consortium on Excitonic Solar Cells, ERC COG:648239, and Royal Society of Chemistry E21-9668828170.

REFERENCES

[1] Guo Q, Hillhouse HW, Agrawal R. Synthesis of Cu2ZnSnS4 Nanocrystal Ink and Its Use for Solar Cells. Journal of the American Chemical Society. 2009;131:11672-3.

[2] Peter LM. Towards sustainable photovoltaics: the search for new materials. Philosophical Transactions of the Royal Society A: Mathematical, Physical and Engineering Sciences. 2011;369:1840-56.

[3] Scragg JJ, Dale PJ, Peter LM. Towards sustainable materials for solar energy conversion: Preparation and photoelectrochemical characterization of Cu2ZnSnS4. Electrochemistry Communications. 2008;10:639-42.

[4] Coughlan C, Ibáñez M, Dobrozhan O, Singh A, Cabot A, Ryan KM. Compound Copper Chalcogenide Nanocrystals. Chemical Reviews. 2017;117:5865-6109.

[5] Tiwari D, Cattelan M, Harniman RL, Sarua A, Fox N, Koehler T, et al. Impact of Sb and Na Doping on the Surface Electronic Landscape of Cu2ZnSnS4 Thin Films. ACS Energy Letters. 2018;3:2977-82.

[6] Tiwari D, Koehler T, Lin X, Harniman R, Griffiths I, Wang L, et al. Cu2ZnSnS4 Thin Films Generated from a Single Solution Based

Precursor: The Effect of Na and Sb Doping. Chemistry of Materials. 2016;28:4991-7.

[7] Wang W, Winkler MT, Gunawan O, Gokmen T, Todorov TK, Zhu Y, et al. Device Characteristics of CZTSSe Thin-Film Solar Cells with 12.6% Efficiency. Advanced Energy Materials. 2014;4:1301465.

[8] Wallace SK, Mitzi DB, Walsh A. The Steady Rise of Kesterite Solar Cells. ACS Energy Letters. 2017;2:776-9.

[9] Bourdais S, Choné C, Delatouche B, Jacob A, Larramona G, Moisan C, et al. Is the Cu/Zn Disorder the Main Culprit for the Voltage Deficit in Kesterite Solar Cells? Advanced Energy Materials. 2016;6:1502276.

[10] Kim S, Park J-S, Walsh A. Identification of Killer Defects in Kesterite Thin-Film Solar Cells. ACS Energy Letters. 2018;3:496-500.

[11] Barkhouse DAR, Gunawan O, Gokmen T, Todorov TK, Mitzi DB. Device characteristics of a 10.1% hydrazine-processed Cu2ZnSn(Se,S)4 solar cell. Progress in Photovoltaics: Research and Applications. 2012;20:6-11.

[12] Park JS, Kim S, Xie Z, Walsh A. Point defect engineering in thin-film solar cells. Nature Reviews Materials. 2018;3:194-210.

[13] Park J-S, Kim S, Walsh A. Stability and electronic properties of planar defects in quaternary I2-II-IV-VI4 semiconductors. Journal of Applied Physics. 2018;124:165705.

[14] Park J-S, Kim S, Hood SN, Walsh A. Open-circuit voltage deficit in Cu2ZnSnS4 solar cells by interface bandgap narrowing. Applied Physics Letters. 2018;113:212103.

[15] Kattan NA, Griffiths IJ, Cherns D, Fermín DJ. Observation of antisite domain boundaries in Cu2ZnSnS4 by atomic-resolution transmission electron microscopy. Nanoscale. 2016;8:14369-73.

[16] Kattan N, Hou B, Fermín DJ, Cherns D. Crystal structure and defects visualization of Cu2ZnSnS4 nanoparticles employing transmission electron microscopy and electron diffraction. Applied Materials Today. 2015;1:52-9.

[17] Chen S, Gong XG, Walsh A, Wei S-H. Crystal and electronic band structure of Cu2ZnSnX4 (X=S and Se) photovoltaic absorbers: First-principles insights. Applied Physics Letters. 2009;94:041903.

[18] Chen S, Walsh A, Yang J-H, Gong XG, Sun L, Yang P-X, et al. Compositional dependence of structural and electronic properties of Cu${}_{2}$ZnSn(S,Se)${}_{4}$ alloys for thin film solar cells. Physical Review B. 2011;83:125201.

[19] [19] Persson C. Electronic and optical properties of Cu2ZnSnS4 and Cu2ZnSnSe4. Journal of Applied Physics. 2010;107:053710.

[20] [20] Walsh A, Chen S, Wei S-H, Gong X-G. Kesterite Thin-Film Solar Cells: Advances in Materials Modelling of Cu2ZnSnS4. Advanced Energy Materials. 2012;2:400-9.

[21] [21] Li J, Mitzi DB, Shenoy VB. Structure and Electronic Properties of Grain Boundaries in Earth-Abundant Photovoltaic Absorber Cu2ZnSnSe4. ACS Nano. 2011;5:8613-9.

[22] [22] Chen S, Walsh A, Gong X-G, Wei S-H. Classification of Lattice Defects in the Kesterite Cu2ZnSnS4 and Cu2ZnSnSe4 Earth-Abundant Solar Cell Absorbers. Advanced Materials. 2013;25:1522-39.

[23] [23] Hou B, Benito-Alifonso D, Kattan N, Cherns D, Galan MC, Fermín DJ. Initial Stages in the Formation of Cu2ZnSn(S,Se)4 Nanoparticles. Chemistry – A European Journal. 2013;19:15847-51.

[24] [24] Hadke S, Huang M, Chen C, Tay YF, Chen S, Tang J, et al. Emerging Chalcogenide Thin Films for Solar Energy Harvesting Devices. Chemical Reviews. 2021.

[25] Hou B, Benito-Alifonso D, Webster RF, Cherns D, Galan MC, Fermín DJ. Synthetic Mechanism Studies of Iron Selenides: An Emerging Class of Materials for Electrocatalysis. Catalysts. 2021;11:681.

[26] Plana D, Humphrey JJL, Bradley KA, Celorrio V, Fermín DJ. Charge Transport Across High Surface Area Metal/Diamond Nanostructured Composites. ACS Applied Materials & Interfaces. 2013;5:2985-90.

[27] Chen F, Qing Q, Xia J, Li J, Tao N. Electrochemical Gate-Controlled Charge Transport in Graphene in Ionic Liquid and Aqueous Solution. Journal of the American Chemical Society. 2009;131:9908-9.

[28] Riha SC, Parkinson BA, Prieto AL. Compositionally Tunable Cu2ZnSn(S1–xSex)4 Nanocrystals: Probing the Effect of Se-Inclusion in Mixed Chalcogenide Thin Films. Journal of the American Chemical Society. 2011;133:15272-5.

[29] Fermín DJ, Ponomarev EA, Peter LM. A kinetic study of CdS photocorrosion by intensity modulated photocurrent and photoelectrochemical impedance spectroscopy. Journal of Electroanalytical Chemistry. 1999;473:192-203.

[30] Scragg JJ, Dale PJ, Peter LM. Synthesis and characterization of Cu2ZnSnS4 absorber layers by an electrodeposition-annealing route. Thin Solid Films. 2009;517:2481-4.